

Constraining the nuclear equation of state with GW170817

Soumi De¹, Daniel Finstad¹, James M. Lattimer², Duncan A. Brown¹, Edo Berger³, and Christopher M. Biwer^{1,4}

¹ *Department of Physics, Syracuse University, Syracuse, NY 13244, USA*

² *Department of Physics and Astronomy, Stony Brook University, Stony Brook, NY 11794-3800, USA*

³ *Harvard-Smithsonian Center for Astrophysics, 60 Garden Street, Cambridge, Massachusetts 02139, USA and*

⁴ *Applied Computer Science (CCS-7), Los Alamos National Laboratory, Los Alamos, NM, 87545, USA*

We use gravitational-wave observations of the binary neutron star merger GW170817 to explore the equation of state of matter at super-nuclear densities. We perform Bayesian parameter estimation with the source location and distance informed by electromagnetic observations. We also assume that the two stars have the same equation of state; we demonstrate that for stars with masses comparable to the component masses of GW170817, this is effectively implemented by assuming that the star's dimensionless tidal deformabilities are determined by the binary's mass ratio q by $\Lambda_1/\Lambda_2 = q^6$. We investigate different choices of prior on the component masses of the neutron stars. We find that the tidal deformability and 90% credible interval is $\tilde{\Lambda} = 310^{+679}_{-234}$ for a uniform component mass prior, $\tilde{\Lambda} = 354^{+691}_{-245}$ for a component mass prior informed by radio observations of Galactic double neutron stars, and $\tilde{\Lambda} = 334^{+669}_{-241}$ for a component mass prior informed by radio pulsars. We find a robust measurement of the common radius of the neutron stars across all mass priors of $8.7 \leq \hat{R} \leq 14.1$ km, with a mean value of $\langle \hat{R} \rangle = 11.5$ km. Our results are the first measurement of tidal deformability with a physical constraint on the star's equation of state and place the first lower bounds on the deformability and radii of neutron stars using gravitational waves.

PACS numbers: 95.85.Sz, 26.60.Kp, 97.80.-d

Introduction—On August 17, 2017 LIGO and Virgo observed gravitational waves from a binary neutron star coalescence, GW170817 [1]. This observation can be used to explore the equation of state (EOS) of matter at super-nuclear densities [2, 3]. This information is encoded as a change in gravitational-wave phase evolution caused by the tidal deformation of the neutron stars [4]. At leading order, the tidal effects are imprinted in the gravitational-wave signal through the binary tidal deformability [4, 5]

$$\tilde{\Lambda} = \frac{16}{13} \frac{(12q + 1)\Lambda_1 + (12 + q)q^4\Lambda_2}{(1 + q)^5}, \quad (1)$$

where $q = m_2/m_1 \leq 1$ is the binary's mass ratio. The deformability of each star is

$$\Lambda_{1,2} = \frac{2}{3} k_2 \left(\frac{R_{1,2} c^2}{G m_{1,2}} \right)^5, \quad (2)$$

where k_2 is the tidal Love number [4, 5], which depends on the star's mass and the EOS. $R_{1,2}$ and $m_{1,2}$ are the radii and masses of the neutron stars, respectively.

In the results of Ref. [1], the priors on $\Lambda_{1,2}$ are taken to be completely uncorrelated, which is equivalent to assuming that each star may have a different EOS. Here, we re-analyze the gravitational-wave data using Bayesian inference [6–8] to measure the tidal deformability, using a correlation between Λ_1 and Λ_2 which follows from the assumption that both stars have the same EOS. We repeat our analysis without the common EOS constraint and calculate the Bayes factor that compares the evidences for these two models. We also fix the sky position and distance from electromagnetic observations [9, 10]. We study the effect of the prior for the component masses by performing analyses with three different priors: the first is uniform between

1 and $2M_\odot$, the second is informed by radio observations of double neutron star binaries, and the third is informed by the masses of isolated pulsars [11].

The common equation of state constraint—To explore imposing a common EOS constraint, we employ a piecewise polytrope scheme [12] to simulate thousands of equations of state. Each EOS obeys causality, connects at low densities to the well-known EOS of neutron star crusts [13], is constrained by experimental and theoretical studies of the symmetry properties of matter near the nuclear saturation density, and satisfies the observational constraint for the maximum mass of a neutron star, $m_{\text{max}} \geq 2M_\odot$ [14]. Fig. 1 shows the results of Tolman-Oppenheimer-Volkoff (TOV) integrations [15] to determine Λ as functions of m , R , and the EOS. Each configuration is color-coded according to its radius. In the relevant mass range, Λ generally varies as m^{-6} . For a given mass m , there is an inherent spread of about a factor ten in Λ , which is correlated with R^6 . We find that the star's tidal deformability is related to its compactness parameter $\beta = Gm/(Rc^2)$ by the relation $\Lambda = a\beta^{-6}$. We find that $a = 0.0093 \pm 0.0007$ bounds this relation if $1.1M_\odot \leq m \leq 1.6M_\odot$ (note that this is a bound, not a confidence interval). The additional power of β^{-1} in the $\Lambda - \beta$ relation, relative to β^{-5} in Eq. (2), originates because the dimensionless tidal Love number, k_2 , varies roughly as β^{-1} for masses $\geq 1M_\odot$, although this is not the case for all masses. For $m \rightarrow 0$ we see that $k_2 \rightarrow 0$ so that k_2 is proportional to β with a positive power, but since neutron stars with $m < 1M_\odot$ are physically unrealistic, that domain is not pertinent in our study.

We observed that, for nearly every specific EOS, the

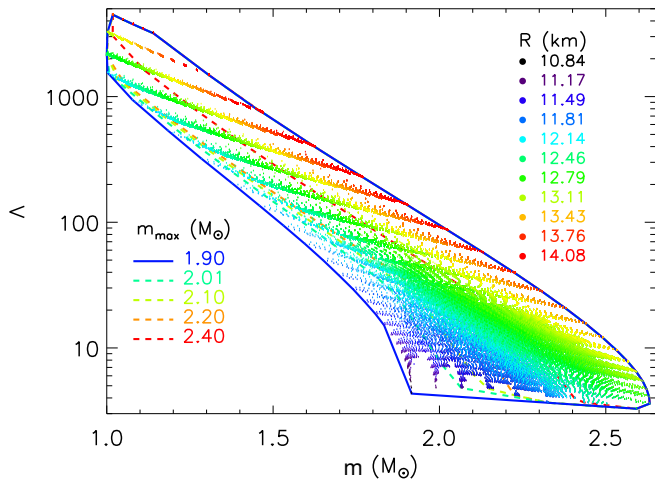


FIG. 1. The tidal deformability Λ as a function of mass for physically realistic polytropes. A TOV integration with each EOS parameter set results in a series of values of $\Lambda(m)$ that are shown as points colored by their radii R . Dashed curves are lower bounds to Λ for a given mass m which vary depending on the assumed lower limit to the neutron star maximum mass, m_{\max} . All values of m_{\max} produce the same upper bound.

range of stellar radii in the mass range of interest for GW170817 is typically small. As long as $m_{\max} \geq 2M_{\odot}$, the piecewise polytrope study reveals $\langle \Delta R \rangle = -0.070$ km and $\sqrt{\langle (\Delta R)^2 \rangle} = 0.11$ km, where $\Delta R \equiv R_{1.6} - R_{1.1}$ with $R_{1.1, 1.6}$ the radii of stars with $m = 1.1M_{\odot}$ and $m = 1.6M_{\odot}$, respectively. Therefore, for masses relevant for GW170817, each EOS assigns a common value of \hat{R} to stellar radii with little sensitivity to the mass. We can hereby combine the relations $\Lambda = a\beta^{-6}$ and $R_1 = R_2$ to find the simple prescription $\Lambda_1 = q^6\Lambda_2$. We impose the common EOS constraint in our analysis using this relation.

Implications for the neutron star radius—The common EOS constraint allows us to show that the binary tidal deformability $\tilde{\Lambda}$ is essentially a function of the chirp mass \mathcal{M} , the common radius \hat{R} , and the mass ratio q , but that its dependence on q is very weak. Substituting the expressions $\Lambda = a\beta^{-6}$ and $R = \hat{R}$ into Eq. (1), we find

$$\tilde{\Lambda} = \frac{16a}{13} \left(\frac{\hat{R}c^2}{GM} \right)^6 f(q). \quad (3)$$

where $f(q)$ is very weakly dependent on q :

$$f(q) = q^{8/5}(12 - 11q + 12q^2)(1 + q)^{-26/5}. \quad (4)$$

For example, if we compare a binary with $q = 0.75$ to an equal mass binary, we find $f(0.75)/f(1) = 1.021$. As long as $q \geq 0.6$, valid for $1M_{\odot} \leq m \leq 1.6M_{\odot}$ for both stars, we infer from Eq. (3),

$$\tilde{\Lambda} = a' \left(\frac{\hat{R}c^2}{GM} \right)^6, \quad (5)$$

where $a' = 0.0042 \pm 0.0004$. The supplemental material shows TOV integrations for a range of EOS that validate this relationship. For stars with masses comparable to GW170817, the common radius \hat{R} can be found from the inversion of Eq. (1),

$$\hat{R} \simeq R_{1.4} \simeq (11.2 \pm 0.2) \frac{\mathcal{M}}{M_{\odot}} \left(\frac{\tilde{\Lambda}}{800} \right)^{1/6} \text{ km}. \quad (6)$$

The quoted errors originate from the uncertainties in a and q , and amount in total to 2%.

Parameter Estimation Methods—We use Bayesian inference to measure the parameters of GW170817 [16]. We calculate the posterior probability density function, $p(\vec{\theta}|\vec{d}(t), H)$, for the set of parameters $\vec{\theta}$ for the gravitational-waveform model, H , given the LIGO Hanford, LIGO Livingston, and Virgo data $\vec{d}(t)$ [17, 18]

$$p(\vec{\theta}|\vec{d}(t), H) = \frac{p(\vec{\theta}|H)p(\vec{d}(t)|\vec{\theta}, H)}{p(\vec{d}(t)|H)}. \quad (7)$$

The prior, $p(\vec{\theta}|H)$, is the set of assumed probability distributions for the waveform parameters. The likelihood $p(\vec{d}(t)|\vec{\theta}, H)$ assumes a Gaussian model for the detector noise [19]. Marginalization of the likelihood to obtain the posterior probabilities is performed using Markov Chain Monte Carlo (MCMC) techniques using the *PyCBC Inference* software [6, 7] and the parallel-tempered *emcee* sampler [8]. We fix the sky location and distance to GW170817 [9, 10] and calculate the posterior probabilities for the remaining source parameters. Following Ref. [1], the waveform model H is the restricted TaylorF2 post-Newtonian aligned-spin model [20]. Technical details of our parameter estimation and a comparison to Fig. 5 of Ref [1] are provided as supplemental materials.

To implement the common EOS constraint we construct the priors on $\Lambda_{1,2}$ according to

$$\Lambda_1 = q^3\Lambda_s, \quad \Lambda_2 = q^{-3}\Lambda_s, \quad (8)$$

where $\Lambda_s \sim U[0, 5000]$. We discard draws with $\tilde{\Lambda} > 5000$, since these values are beyond the range of all plausible EOS. The resulting prior on $\tilde{\Lambda}$ is uniform between 0 and 5000. We also perform analyses that do not assume the common EOS constraint where we allow completely uncorrelated priors for $\Lambda_{1,2}$. This allows us to compare the evidences between these hypotheses. For the uncorrelated $\Lambda_{1,2}$ analyses, the prior for $\Lambda_1 \sim U[0, 1000]$ and $\Lambda_2 \sim U[0, 5000]$ with these intervals set by the range of plausible equations of state in the mass range of interest, our convention of $m_1 \geq m_2$, and discarding draws with $\tilde{\Lambda} > 5000$.

The choice of mass prior can have an impact on the recovery of the tidal deformability [21]. To investigate this, we carry out our parameter estimation analyses using three different priors on the binary's component masses. We first

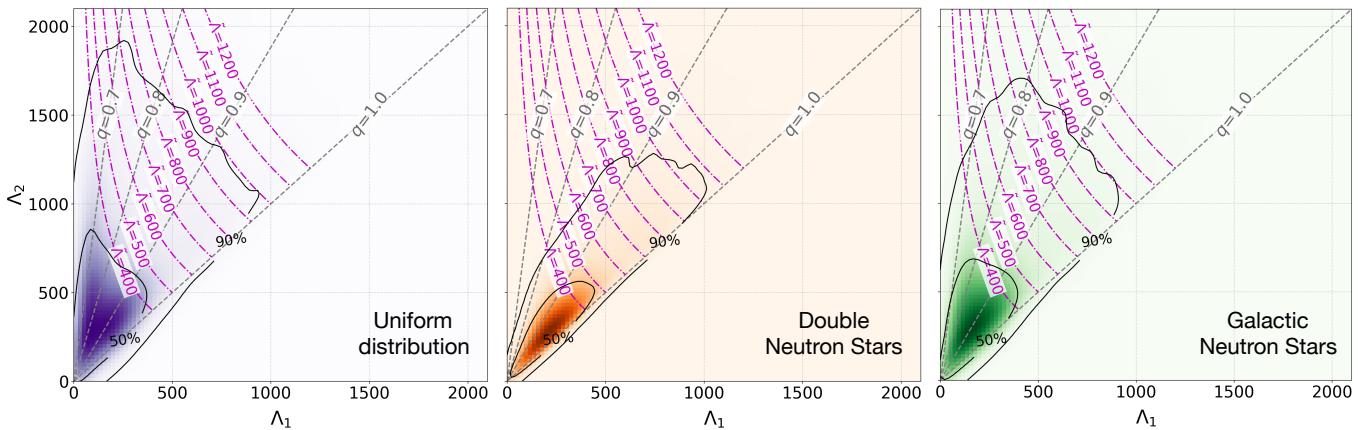


FIG. 2. Posterior probability densities for $\Lambda_{1,2}$ with the common EOS constraint using Uniform (left), Double Neutron Stars (middle), and Galactic Neutron Stars (right) component mass priors. The 50% and 90% credible region contours are shown as solid curves. Overlaid are contours of $\tilde{\Lambda}$ (in magenta) and q (in gray).

assume a uniform prior on each star’s mass, with $m_{1,2} \sim U[1, 2] M_{\odot}$. We then assume a Gaussian prior on the component masses $m_{1,2} \sim N(\mu = 1.33, \sigma = 0.09) M_{\odot}$, which is a fit to masses of neutron stars observed in double neutron star systems [11]. The third prior assumes that the component masses are drawn from a fit to the observed mass distributions of recycled and slow pulsars in the Galaxy with $m_1 \sim N(\mu = 1.54, \sigma = 0.23) M_{\odot}$ and $m_2 \sim N(\mu = 1.49, \sigma = 0.19) M_{\odot}$ [11]. We impose the constraint $m_1 \geq m_2$ which leads to $\Lambda_2 \geq \Lambda_1$. For all our analyses, the prior on the component spins is $\chi_{1,2} \sim U[-0.05, 0.05]$, consistent with the expected spins of field binaries when they enter the LIGO-Virgo sensitive band [22].

Results—The full posterior probability densities for the parameters $p(\vec{\theta}|\vec{d}(t), H)$ for each of our MCMC runs are shown in the supplemental materials and are available for download at Ref. [23]. Fig. 2 shows the posterior probability densities for Λ_1 and Λ_2 with 90% and 50% credible region contours. Overlaid are q contours and $\tilde{\Lambda}$ contours obtained from Eq. (1), $\Lambda = a\beta^{-6}$, and $R_1 \simeq R_2 \simeq \hat{R}$ as

$$\Lambda_1(\tilde{\Lambda}, q) = \frac{13}{16} \tilde{\Lambda} \frac{q^2(1+q)^4}{12q^2 - 11q + 12}, \quad \Lambda_2(\tilde{\Lambda}, q) = q^{-6} \Lambda_1 \quad (9)$$

Due to our constraint $\Lambda_2 \geq \Lambda_1$, our credible contours are confined to the region where $q \leq 1$. One can easily demonstrate that $\Lambda_2 \geq \Lambda_1$ is valid unless $(c^2/G)dR/dm > 1$, which is impossible for realistic equations of state. For the entire set of piecewise polytropes satisfying $m_{\max} > 2M_{\odot}$ we considered, $(c^2/G)dR/dm$ never exceeded 0.26. Even if a first order phase transition appeared in stars with masses between m_2 and m_1 , it would be necessarily true that $dR/dm < 0$ across the transition. Due to the q dependence of Λ_1 , Λ_2 , the credible region enclosed by the contours broadens from the double neutron star (most restricted), to the pulsar, to the uniform mass (least restricted)

priors. However, the upper bound of the credible region is robust.

Using Eq. 6, we map our \mathcal{M} and $\tilde{\Lambda}$ posteriors to $\hat{R} \simeq R_{1.4}$ posteriors, allowing us to estimate the common radius of the neutron stars for GW170817 for each mass prior. Fig. 3 shows the posterior probability distribution for the binary tidal deformability $\tilde{\Lambda}$ and the common radius \hat{R} of the neutron stars in the binary. We find $\tilde{\Lambda} = 310^{+679}_{-234}$ for the uniform component mass prior, $\tilde{\Lambda} = 354^{+691}_{-245}$ for the prior informed by double neutron star binaries in the Galaxy, and $\tilde{\Lambda} = 334^{+669}_{-241}$ for the prior informed by all Galactic neutron star masses (errors represent 90% credible intervals). Our measurement of $\tilde{\Lambda}$ appears to be robust to the choice of component mass prior, within the (relatively large) statistical errors on its measurement. Our results suggest a radius $\hat{R} = 11.3^{+2.4}_{-2.4} \pm 0.2$ km (90% credible interval, statistical and systematic errors) for the uniform mass prior, $\hat{R} = 11.6^{+2.3}_{-2.1} \pm 0.2$ km for double neutron star mass prior, and $\hat{R} = 11.5^{+2.3}_{-2.2} \pm 0.2$ km for the prior based on all neutron star masses.

We repeat our analysis for each mass prior without the common EOS constraint and calculate the Bayes factor—the ratio of the evidences $p(\vec{d}(t)|H)$ —between the common EOS constrained and unconstrained analyses. We find Bayes factors \mathcal{B} of 525, 230, and 285 for the three mass priors, respectively, indicating that the data strongly favors the common EOS constraint in all cases. The Bayes factors comparing the evidence from the three mass priors are of order unity, so we cannot claim any preference between the mass priors. For the uniform mass prior, we computed the Bayes factor that compares a model with a prior $\Lambda_s \sim U[0, 5000]$ to a model with a prior $\Lambda_s \sim U[0, 100]$. We find $\log \mathcal{B} \sim 1$, suggesting that the data favors a model that includes measurement of tidal deformability $\tilde{\Lambda} \gtrsim 100$. However, the evidences were calculated using thermody-

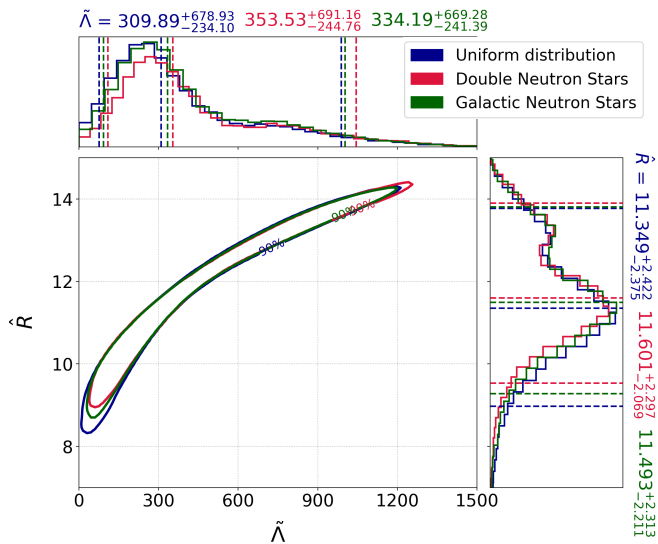


FIG. 3. The 90% credible region of the posterior probability for the common radius \hat{R} and binary tidal deformability $\tilde{\Lambda}$ with the common EOS constraint for the three mass priors. The posteriors for the individual parameters are shown with dotted lines at the 5%, 50% and 95% percentiles.

numeric integration of the MCMC chains [8] and we will investigate model selection using e.g. nested sampling [24] in a future work.

Finally, we note the post-Newtonian waveform family used will result in systematic errors in our measurement of the tidal deformability [25, 26]. However, this waveform family allows a direct comparison to the results of Ref. [1]. Accurate modeling of the waveform is challenging, as the errors in numerical simulations are comparable to the size of the matter effects that we are trying to measure [27]. Waveform systematics and comparison of other waveform models (e.g. [28]) will be investigated in a future work.

Discussion—Using Bayesian parameter estimation we have measured the tidal deformability and common radius of the neutron stars in GW170817. Table I summarizes our findings. To compare to Ref. [1], which reports a 90% upper limit on $\tilde{\Lambda} \leq 800$ under the assumption of a uniform prior on $\tilde{\Lambda}$, we integrate the posterior for $\tilde{\Lambda}$ to obtain 90% upper limits on $\tilde{\Lambda}$. For the common EOS analyses these are 825, 888, and 852 for the uniform, double neutron star, and Galactic neutron star component mass priors, respectively. The difference between our results for the three mass priors is consistent with the physics of the gravitational waveform. At constant chirp mass, decreasing q causes the binary to inspiral more quickly [29]. At constant chirp mass and constant q , increasing $\tilde{\Lambda}$ also causes the binary to inspiral more quickly, so there is a mild degeneracy between q and $\tilde{\Lambda}$. The uniform mass prior allows the largest range of mass ratios, so we can fit the data with a larger q and smaller $\tilde{\Lambda}$. The double neutron star mass prior allows the smallest range of mass ratios and so a larger $\tilde{\Lambda}$ is required

Mass prior	$\tilde{\Lambda}$	\hat{R} (km)	\mathcal{B}	$\tilde{\Lambda}_{90\%}$
Uniform	310^{+679}_{-234}	$11.3^{+2.4}_{-2.4} \pm 0.2$	525	< 825
Double neutron star	354^{+691}_{-245}	$11.6^{+2.3}_{-2.1} \pm 0.2$	230	< 852
Galactic neutron star	334^{+669}_{-241}	$11.5^{+2.3}_{-2.2} \pm 0.2$	285	< 888

TABLE I. Results from parameter estimation analyses using three different mass prior choices with the common EOS constraint. We show 90% credible intervals for $\tilde{\Lambda}$, 90% credible intervals and systematic errors for \hat{R} , Bayes factors \mathcal{B} comparing our common EOS to the unconstrained results, and the 90% upper limits on $\tilde{\Lambda}$.

to fit the data, with the Galactic neutron star mass prior lying between these two cases.

Nevertheless, considering all analyses we performed with different mass prior choices, we find a relatively robust measurement of the common neutron star radius with a mean value $\langle \hat{R} \rangle = 11.5$ km bounded above by $\hat{R} < 14.1$ km and below by $\hat{R} > 8.8$ km. Nuclear theory and experiment currently predict a somewhat smaller range by 2 km, but with approximately the same centroid as our results. Ref. [11] used results from 12 photospheric radius expansion measurements of X-ray binaries to obtain $R = 10.6 \pm 0.6$, however this result neglects systematic uncertainties which could be 2 km or greater.

In this *letter*, we have shown that for binary neutron star mergers consistent with observed double neutron star systems, assuming a common EOS implies that $\Lambda_1/\Lambda_2 \simeq q^6$. We find evidence from GW170817 that favors the common EOS interpretation compared to uncorrelated deformabilities. Variation of the component mass priors does not significantly influence our conclusions, suggesting that our results are robust. The lower limits of all our 90% credible intervals lie above 75, which is larger than the lower causal limit on $\tilde{\Lambda} \geq 65$ for a binary with $\mathcal{M} = 1.19 M_\odot$ and $m_{\max} > 2 M_\odot$ [12]. Our results support the conclusion that we find the first evidence for finite size effects using gravitational-wave observations.

Acknowledgements—We thank Stefan Ballmer, Swetha Bhagwat, Steven Reyes, Andrew Steiner, and Douglas Swesty for helpful discussions. We particularly thank Collin Capano and Alexander Nitz for contributing to the development of PyCBC Inference; however, they did not wish to be authors due to restrictions placed by LIGO Scientific Collaboration policies. This work was supported by NSF awards PHY-1404395 (DAB, CMB), PHY-1707954 (DAB, SD, DF), AST-1714498 (EB), and DOE Award DE-FG02-87ER40317 (JML). Computations were supported by Syracuse University and NSF award OAC-1541396. DAB, EB, SD, and JML thank Kavli Institute for Theoretical Physics which is supported by the NSF award PHY-1748958. The gravitational-wave data used in this work was obtained from the LIGO Open Science Center. LOSC is a service of LIGO Laboratory, the LIGO Scientific Collaboration and the Virgo Collaboration.

-
- [1] B. Abbott *et al.*, Phys. Rev. Lett. **119**, 161101 (2017).
 - [2] K. S. Thorne, in *Three hundred years of gravitation*, edited by S. W. Hawking and W. Israel (Cambridge University Press, Cambridge, 1987) Chap. 9, pp. 330–458.
 - [3] J. S. Read *et al.*, Phys. Rev. **D79**, 124033 (2009).
 - [4] E. E. Flanagan and T. Hinderer, Phys. Rev. **D77**, 021502 (2008).
 - [5] T. Hinderer, Astrophys. J. **677**, 1216 (2008).
 - [6] C. M. Biwer, C. Capano, *et al.*, (In preparation.).
 - [7] A. Nitz *et al.*, *PyCBC v1.9.4* (2018).
 - [8] D. Foreman-Mackey *et al.*, PASP **125**, 306 (2013).
 - [9] M. Soares-Santos *et al.*, Astrophys. J. **848**, L16 (2017).
 - [10] M. Cantiello *et al.*, Astrophys. J. **854**, L31 (2018).
 - [11] F. Özel and P. Freire, Ann. Rev. Astron. Astrophys. **54**, 401 (2016).
 - [12] J. M. Lattimer and M. Prakash, Phys. Rept. **621**, 127 (2016).
 - [13] J. M. Lattimer, Ann. Rev. Nucl. Part. Sci. **62**, 485 (2012).
 - [14] J. Antoniadis *et al.*, Science **340**, 6131 (2013).
 - [15] J. R. Oppenheimer and G. M. Volkoff, Phys. Rev. **55**, 374 (1939).
 - [16] N. Christensen and R. Meyer, Phys. Rev. **D64**, 022001 (2001).
 - [17] M. Vallisneri *et al.*, J. Phys. Conf. Ser. **610**, 012021 (2015).
 - [18] K. Blackburn *et al.*, *LOSC CLN Data Products for GW170817* (2017).
 - [19] C. Rover *et al.*, Phys. Rev. **D75**, 062004 (2007).
 - [20] B. S. Sathyaprakash and S. V. Dhurandhar, Phys. Rev. **D44**, 3819 (1991).
 - [21] M. Agathos *et al.*, Phys. Rev. **D92**, 023012 (2015).
 - [22] D. A. Brown *et al.*, Phys. Rev. **D86**, 084017 (2012).
 - [23] S. De *et al.*, *SUGWG GitHub Repository* (2018).
 - [24] J. Skilling, Bayesian Anal. **1**, 833 (2006).
 - [25] L. Wade *et al.*, Phys. Rev. **D89**, 103012 (2014).
 - [26] B. D. Lackey and L. Wade, Phys. Rev. **D91**, 043002 (2015).
 - [27] K. Barkett *et al.*, Phys. Rev. **D93**, 044064 (2016).
 - [28] S. Bernuzzi *et al.*, Phys. Rev. Lett. **114**, 161103 (2015).
 - [29] M. Hannam *et al.*, Astrophys. J. **766**, L14 (2013).

Supplemental Material

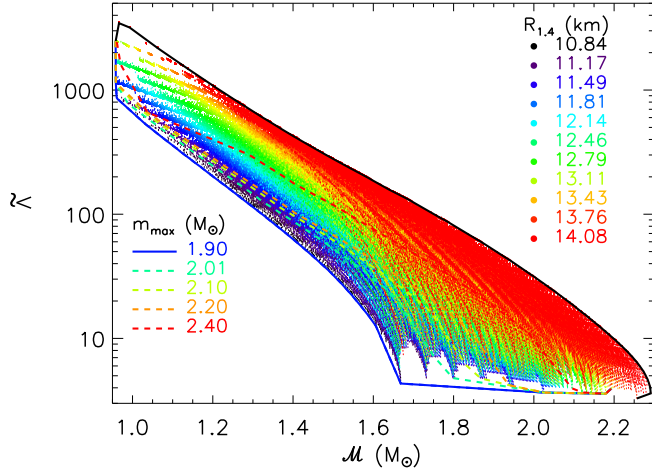


FIG. 1. The dimensionless binary tidal deformability $\tilde{\Lambda}$ as a function of chirp mass \mathcal{M} for piecewise polytropes with parameters bounded by causality, neutron matter studies and nuclear experiments. Various binary mass combinations with each equation of state result in many points which are color-coded according to that equation of state's value of $R_{1.4}$. The values of $\tilde{\Lambda}(\mathcal{M})$ are bounded according to the assumed value of the maximum neutron star mass, m_{\max} .

The common neutron star radius—To validate the relationship

$$\tilde{\Lambda} = a' \left(\frac{\hat{R}c^2}{GM} \right)^6, \quad (1)$$

where $a' = 0.0042 \pm 0.0004$, we perform Tolman-Oppenheimer-Volkoff (TOV) integrations [1] as described in the main text. The relationship between $\tilde{\Lambda}$, chirp mass \mathcal{M} and the common radius \hat{R} closely resembles the relation between Λ , the neutron star mass m and radius R . We confirm this using piecewise polytropes as shown in Fig. 1, which was prepared using the results computed to create Fig. 1 in the main paper. A single mass-radius curve is generated for each equation of state containing N masses between $1M_{\odot}$ and m_{\max} for that EOS. $N(N-1)$ values of $\tilde{\Lambda}$ and \mathcal{M} are then computed for all the unique combinations of m_1 and m_2 from these N masses. The resulting points are plotted in Fig. 2, and are color-coded by that equation of state's value of $R_{1.4}$. The process is repeated for all combinations of the parameters controlling the piecewise polytropic EOS described in [2]. For the entries bounded by $0.9M_{\odot} \leq \mathcal{M} \leq 1.3M_{\odot}$, an interval including GW170817, Eq. (1) is determined by finding the upper and lower bounds of $a' = \tilde{\Lambda}[GM/(R_{1.4}c^2)]^6$.

The numerical results also confirmed our value for a' . This is valid for values of $\mathcal{M} < 1.3M_{\odot}$, which is rele-

vant not only for GW170817 but also for all known double neutron star binaries, which are clustered in the narrow range $1.09M_{\odot} < \mathcal{M} < 1.25M_{\odot}$ [3–5]. The robustness of $\tilde{\Lambda} \propto \beta^{-6}$ confirms that the assumption $R_1 = R_2$ is a valid proposition.

Parameter estimation methods—To measure the source parameters for GW170817, we performed parameter estimation on the Advanced LIGO-Virgo data available at the LIGO Open Science Center [6, 7]. Our analysis was performed with the *PyCBC Inference* software [8, 9] and the parallel-tempered *emcee* sampler [10] for sampling over the parameter space using Markov Chain Monte Carlo (MCMC) techniques [11].

The LOSC data files include a post-processing noise subtraction performed by the LIGO-Virgo Collaboration [7, 12]. The LOSC documentation states that these data have been truncated to remove tapering effects due to the cleaning process [7], however the LOSC data shows evidence of tapering after GPS time 1187008900 in the LIGO Hanford detector. To avoid any contamination of our results we do not use any data after GPS time 1187008891. The power spectral density (PSD) used to construct the likelihood was calculated using Welch's method [13] with 16 second Hann-windowed segments (overlapped by 8 s) taken from GPS time 1187007048 to 1187008680. The PSD estimate is truncated to 8 s length in the time domain using the method described in Ref. [14]. The gravitational-wave data used in the likelihood is taken from the interval 1187008763 to 1187008891. The likelihood is evaluated from a low-frequency cutoff of 25 Hz to the Nyquist frequency of 2048 Hz.

The templates for the waveforms used in our parameter estimation analysis are generated using the restricted TaylorF2 waveform model, a Fourier domain waveform model generated using stationary phase approximation. We use the implementation from the LIGO Algorithm Library (LAL) [15] accurate to 3.5 post-Newtonian (pN) order in orbital phase [16], 2.0 pN order in spin-spin, quadrupole-monopole and self-spin interactions [17, 18], and 3.5 pN order in spin-orbit interactions [19]. The tidal corrections enter at the 5 pN and 6 pN orders [20]. The waveforms are terminated at twice the orbital frequency of a test particle at the innermost stable circular orbit of a Schwarzschild black hole of mass $M = m_1 + m_2$, where $m_{1,2}$ are the masses of the binary's component stars. The TaylorF2 model assumes that the spins of the neutron stars are aligned with the orbital angular momentum. Binary neutron stars formed in the field are expected to have small spins, and precession of the binary's orbital plane is not significant [21].

We fix the sky location of the binary to the right ascension (RA) and declination (Dec) to RA = 197.450374°,

Dec = -23.381495° [22] for all of our runs. We also fix the luminosity distance of NGC 4993 $d_L = 40.7$ Mpc [23]. The small error in the known distance of NGC 4993 produces errors that are much smaller than the errors in measuring the tidal deformability, so fixing this parameter does not affect our conclusions. The MCMC computes the marginalized posterior probabilities for the remaining source parameters: chirp mass \mathcal{M} , mass ratio q , the component (aligned) spins $\chi_{1,2} = cJ_{1,2}/Gm_{1,2}^2$, component tidal deformabilities $\Lambda_{1,2}$, polarization angle ψ , inclination angle ι , coalescence phase ϕ_c , and coalescence time t_c . When generating the waveform in the MCMC, each $m_{1,2}$ draws follow the constraint $m_1 \geq m_2$, and the masses are transformed to the detector frame chirp mass \mathcal{M}^{det} and q with a restriction $1.1876 \leq \mathcal{M}^{\text{det}} \leq 1.2076$.

For direct comparison with the results of Ref. [24], Fig 2 shows the posterior probability densities for $\Lambda_{1,2}$ for an MCMC using the above configuration for the uniform component mass prior $m_{1,2} \sim U[1, 2] M_\odot$, and assuming that the priors on $\Lambda_{1,2}$ are completely uncorrelated ($\Lambda_{1,2} \sim U[0, 3000]$). No cut is placed on $\tilde{\Lambda}$ in this analysis. We have digitized the 50% and 90% contours from Fig. 5 of Ref. [24] and compared them to 50% and 90% upper limit contours for our result computed using a radial binning to enclose 50% and 90% of the posterior probability starting from $\Lambda_1 = \Lambda_2 = 0$. The 90% contours agree well, with a slight difference in the 50% contours. Given the accuracy of measuring the tidal deformability, this difference can be attributed to small differences in the technical as-

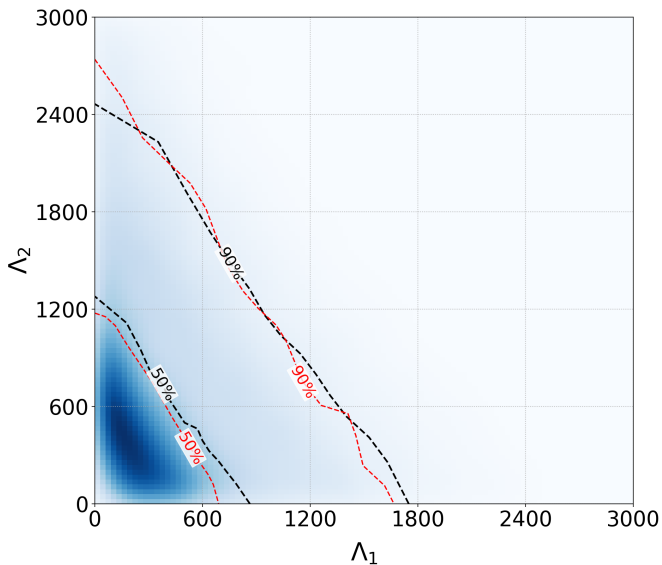


FIG. 2. Posterior probability density function for Λ_1, Λ_2 from unconstrained $\Lambda_{1,2} \sim U[0, 3000]$, $m_{1,2} \sim U[1, 2] M_\odot$, $1.1876 \leq \mathcal{M} \leq 1.2076$, $m_1 \geq m_2$ analysis. The black dotted lines show 50% and 90% upper limits from our analysis. The red dotted lines show 50% and 90% upper limits from the LIGO-Virgo analysis [24].

pects of our analysis compared to that of Ref. [24]. We note that the 90% confidence contour of Fig. 5 in Ref. [24] with $\Lambda_1 = \Lambda_2$, passes through $\tilde{\Lambda} \approx 1100$. If we impose $\Lambda_1 = q^6 \Lambda_2$, then this contour continues to follow $\tilde{\Lambda} \approx 1100$ for $q \leq 1$. We interpret the difference between this result and the result of Table I of Ref. [24] $\tilde{\Lambda} \leq 800$ (90% confidence) as being due to a different choice of prior on $\tilde{\Lambda}$ (one non-uniform and one uniform).

Our common equation of state constraint is implemented in the MCMC by drawing a variable $\Lambda_s \sim U[0, 5000]$, drawing the component masses from their respective priors and computing

$$\Lambda_1 = q^3 \Lambda_s, \quad \Lambda_2 = q^{-3} \Lambda_s, \quad (2)$$

with draws that have $\tilde{\Lambda} > 5000$ discarded. This produces a prior that is uniform in $\tilde{\Lambda}$ between 0 and 5000, as shown in Fig. 3 for all of our three mass priors discussed in the main text. For comparison, we also show the prior on $\tilde{\Lambda}$ computed assuming independent $\Lambda_{1,2} \sim U[0, 3000]$ and the component mass prior $m_{1,2} \sim U[1, 2] M_\odot$. It can be seen that this prior vanishes as $\tilde{\Lambda} \rightarrow 0$ and so can bias the posterior at low values of $\tilde{\Lambda}$. In addition to the physical requirement of a common EOS constraint, the prior used in the common EOS analysis is uniform as $\tilde{\Lambda} \rightarrow 0$, allowing us to fully explore likelihoods in this region, and set lower bounds on our credible intervals.

Results—Fig. 4 shows the posterior probability densities for the parameters of interest in our study: the source frame chirp mass \mathcal{M}^{src} ; the mass ratio $q = m_2/m_1$; the

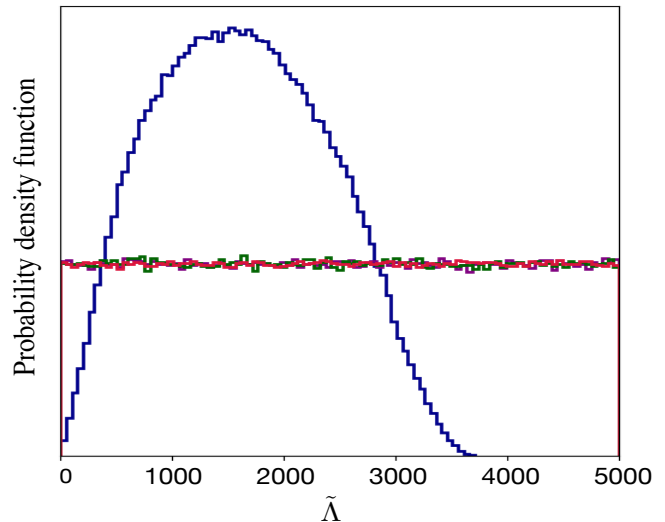


FIG. 3. Comparison of the prior probability distributions on $\tilde{\Lambda}$ for the three mass priors imposing the common EOS constraint: uniform (purple), galactic neutron stars (green), double neutron stars (red) with a prior in $\Lambda_{1,2} \sim U[0, 3000]$ and $m_{1,2} \sim U[1, 2] M_\odot$, $m_1 \geq m_2$ without the common EOS constraint (blue). The priors in the common EOS analysis are uniform across the region of interest.

source frame component masses $m_{1,2}^{\text{src}}$ (which are functions of \mathcal{M}^{src} and q); the effective spin $\chi_{\text{eff}} = m_1\chi_1 + m_2\chi_2/(m_1 + m_2)$; and $\hat{\Lambda}$, the binary tidal deformability. Posterior probability densities are shown for each of the three mass priors with the common EOS constraint imposed, as discussed in the main paper. Electronic files containing the thinned posterior probability densities and an IPython notebook [25] for manipulating these data are available at Ref. [26].

-
- [1] J. R. Oppenheimer and G. M. Volkoff, *Phys. Rev.* **55**, 374 (1939).
- [2] J. M. Lattimer and M. Prakash, *Phys. Rept.* **621**, 127 (2016).
- [3] T. M. Tauris *et al.*, *Astrophys. J.* **846**, 170 (2017), arXiv:1706.09438 [astro-ph.HE].
- [4] F. Özel and P. Freire, *Ann. Rev. Astron. Astrophys.* **54**, 401 (2016).
- [5] J. M. Lattimer, *Ann. Rev. Nucl. Part. Sci.* **62**, 485 (2012).
- [6] M. Vallisneri *et al.*, *J. Phys. Conf. Ser.* **610**, 012021 (2015).
- [7] K. Blackburn *et al.*, *LOSC CLN Data Products for GW170817* (2017).
- [8] C. M. Biwer, C. Capano, *et al.*, (In preparation.).
- [9] A. Nitz *et al.*, *PyCBC v1.9.4* (2018).
- [10] D. Foreman-Mackey *et al.*, *PASP* **125**, 306 (2013).
- [11] W. J. Goodman J., *Commun. Appl. Math. Comput. Sci.* **5**, 65 (2010).
- [12] J. Driggers, S. Vitale, A. Lundgren, M. Evans, K. Kawabe, S. Dwyer, K. Izumi, and P. Fritschel, “Offline noise subtraction for Advanced LIGO,” (2017), <https://dcc.ligo.org/LIGO-P1700260/public>.
- [13] P. Welch, *IEEE Transactions on Audio and Electroacoustics* **15**, 70 (1967).
- [14] B. Allen, W. G. Anderson, P. R. Brady, D. A. Brown, and J. D. E. Creighton, *Phys. Rev.* **D85**, 122006 (2012).
- [15] R. A. Mercer *et al.*, “LIGO Algorithm Library,” (2017), <https://git.ligo.org/lscsoft/lalsuite>.
- [16] A. Buonanno *et al.*, *Phys. Rev.* **D80**, 084043 (2009).
- [17] K. G. Arun *et al.*, *Phys. Rev.* **D79**, 104023 (2009), [Erratum: *Phys. Rev.* **D84**, 049901 (2011)].
- [18] B. Mikoczi, M. Vasuth, and L. A. Gergely, *Phys. Rev.* **D71**, 124043 (2005).
- [19] A. Bohe, S. Marsat, and L. Blanchet, *Class. Quant. Grav.* **30**, 135009 (2013).
- [20] J. Vines, E. Flanagan, and T. Hinderer, *Phys. Rev.* **D83**, 084051 (2011).
- [21] D. A. Brown *et al.*, *Phys. Rev.* **D86**, 084017 (2012).
- [22] M. Soares-Santos *et al.*, *Astrophys. J.* **848**, L16 (2017).
- [23] M. Cantiello *et al.*, *Astrophys. J.* **854**, L31 (2018).
- [24] B. Abbott *et al.*, *Phys. Rev. Lett.* **119**, 161101 (2017).
- [25] F. Pérez and B. E. Granger, *Computing in Science and Engineering* **9**, 21 (2007).
- [26] S. De *et al.*, *SUGWG GitHub Repository* (2018).

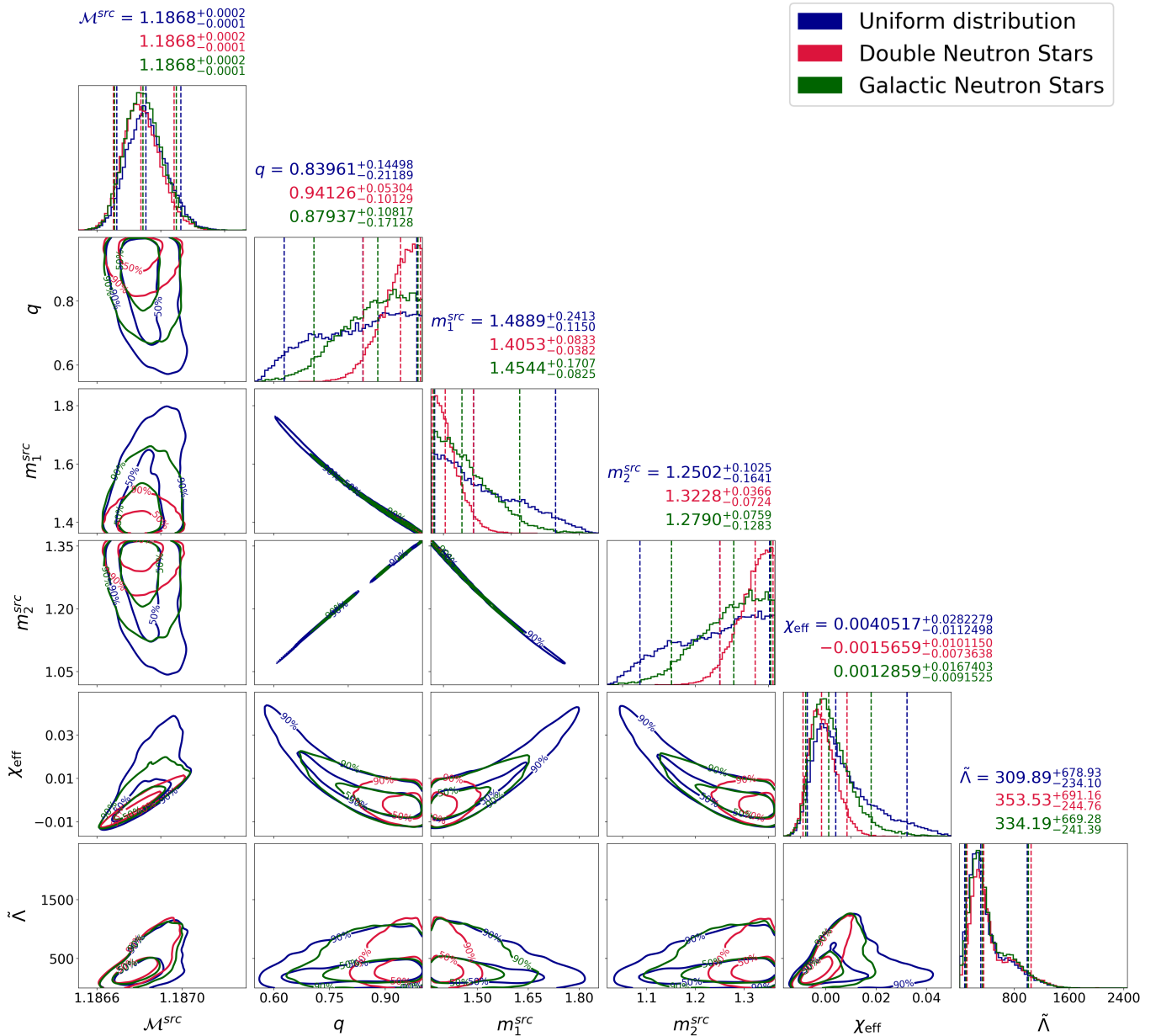


FIG. 4. Posterior distributions for the source frame chirp mass \mathcal{M}^{src} , mass ratio q , source frame primary mass m_1^{src} and secondary mass m_2^{src} , effective spin χ_{eff} , and binary deformability parameter $\tilde{\Lambda}$ from parameter estimation analyses with three different choices of mass priors. The posteriors represented in blue are from the analysis using a uniform prior on component masses, $m_{1,2} \sim U[1, 2] M_{\odot}$. The posteriors represented in red are from the analysis using a Gaussian mass prior for component masses $m_{1,2} \sim N(\mu = 1.33, \sigma = 0.09) M_{\odot}$ known from radio observations of neutron stars in double neutron star (DNS) systems. The posteriors represented in green are from the analysis using the observed mass distributions of recycled and slow pulsars in the Galaxy with $m_1 \sim N(\mu = 1.54, \sigma = 0.23) M_{\odot}$ and $m_2 \sim N(\mu = 1.49, \sigma = 0.19) M_{\odot}$ [4]. All three analyses had the common EOS constraint imposed. The one-dimensional plots show marginalized probability density functions for the parameters. The dashed lines on the one-dimensional histograms represent the 5%, 50% and 95% percentiles for each analysis, the values of which are quoted in the titles of the histograms. The 2D plots show 50% and 90% credible regions for the different pairs of parameters.